Available online at www.sciencedirect.com
ScienceDirect
Journal of Bionic Engineering 12 (2015) 339–351

Effect of Hind Leg Morphology on Performance of a Canine-inspired Quadrupedal Robot

James Andrew Smith, Jamil Jivraj

Ryerson University, 350 *Victoria St*., *Toronto*, *ON*, *Canada*

Abstract

Biomimetic leg designs often appear to be arbitrarily chosen. To make a more objective choice regarding biomimetic leg configuration for small canine-inspired robots, we compare one hind leg to the same leg arranged in a different orientation, and show that the less biomimetic leg provides better performance. This differently-oriented leg design, which we call "transverse-mirrored" was more efficient and faster, both in simulation and experiment even though both leg configurations used the same passive and active components, rest angles, and monoarticular knee spring. In experiments the normal configuration had a maximum speed of 0.33 $m{\cdot}s^{-1}$ and a specific resistance of 5.1. Conversely, the less biomimetic transverse-mirrored configuration had a maximum speed of 0.4 $m{\cdot}s^{-1}$ and specific resistance of 3.9. Therefore the transverse-mirrored leg's best performance yields a 21% increase in speed and 24% decrease in specific resistance when compared to the best performance achieved in the normal biomimetic leg. The major underlying reason is that the knee spring engages more readily in the transverse-mirrored configuration, resulting in this faster and more efficient locomotion. The conclusion is that simply copying from nature does not lead to optimal performance and that insight into the role played by passive design components on natural locomotory dynamics is important.

Keywords: biomimetic, legged robot, quadruped, leg design, walking, legged locomotion

doi: 10.1016/S1672-6529(14)60126-8

1 Introduction

Biologists and biomechanicists have speculated on the effect that leg joint direction plays on the dynamics of locomotion, but validating theories on animals would be difficult or impossible. Unfortunately, roboticists working on bioinspired legged robots have had the opportunity to explore this issue but have, instead, often typically made arbitrary choices when it comes to leg joint direction designs, with potentially significant effects on the robot's natural dynamics[1–4]. Typically, a designer examines a biological leg and extracts a simplified topology as the focus for robot design, such as that seen in Fig. 1. For instance, many robots have been designed with posterior-pointing knees, including Tekken[5], the Jena Hopper[6], KOLT[7,8] and Pfeifer and Iida's quadruped[9]. The Boston Dynamics BigDog has alternated the knee directions[10], without explanation. In monopods it is possible that leg shape, and in particular a bow-like shape, can reduce limb stiffness and leg force[11]. The quadrupedal Biosbot, with two-segment legs and reconfigurable knees[12,13] initially attempted to examine the effect of knee direction on gait performance in a quadruped but the results were insufficiently detailed to draw meaningful conclusions. In contrast, this paper presents, for the first time, detailed simulation and experimental evidence for how the knee direction of a hind leg influences the robot's natural dynamics and subsequently the performance of a walking gait. In short, we find that an inverted leg configuration yields higher speeds and improved energy efficiency.

This work stands out from other studies in leg robotics in the comparisons between simulation and experimentation in legged-robotics studies (*e.g*. Refs. [14–19]) which are rare within the robotics community. Typically, either only experimental results are given, (*e.g*. Refs. [9, 20, 21]) or only simulation results, (*e.g*. Refs. [22–25]) but not both. Given that qualitatively similar results are found both in simulation and experiments of this study we are confident that the improved

Corresponding author: James Andrew Smith
E-mail: jasmith@ryerson.ca

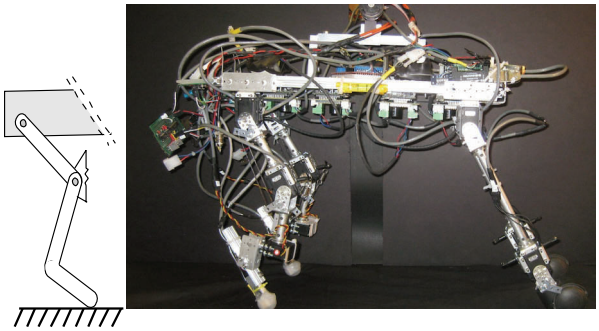

(a) Normal hind leg

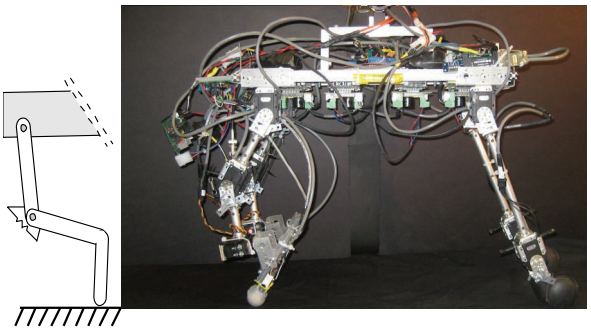

(b) Transverse-mirrored hind leg

Fig. 1 The GARP-5 robot in the (a) normal and (b) transverse-mirrored hind leg configurations.

performance observed using the inverted leg configuration is valid.

2 GARP-5's canine-inspired design

The main objective of this study is to quantify the difference in robot walking performance resulting from varied hind leg configurations. Specifically, we examine the effect played by having knees pointing posteriorly compared to posteriorly on the same bioinspired quadrupedal robot.

The GARP-5 robot, with an effective mass of 1.56 kg, is supported by a boom, shown in Fig. 2. The boom's mass is 1.1 kg, and its counterweight is 6.72 kg. It is common practice for experimental legged robotics to be supported or constrained by booms in order to study the movements of the robot. Booms are used to support the robot in two ways: by allowing the robot to rotate in a circular path of a fixed diameter (rotational booms) or keeping the robot in one spot, such as jumping up and down, or walking on a treadmill (stationary booms). Robots that use rotational booms include Cheetah[26], Raibert's monopod and biped robots[27], Thumper and MABEL robots[28], RABBIT[29], and Run Bot[30]. Robots that are supported by stationary booms include the Jena Walker[31], KOLT[8], and Ernie[32]. The boom was configured to gather angle/position data but not reaction force or torque data.

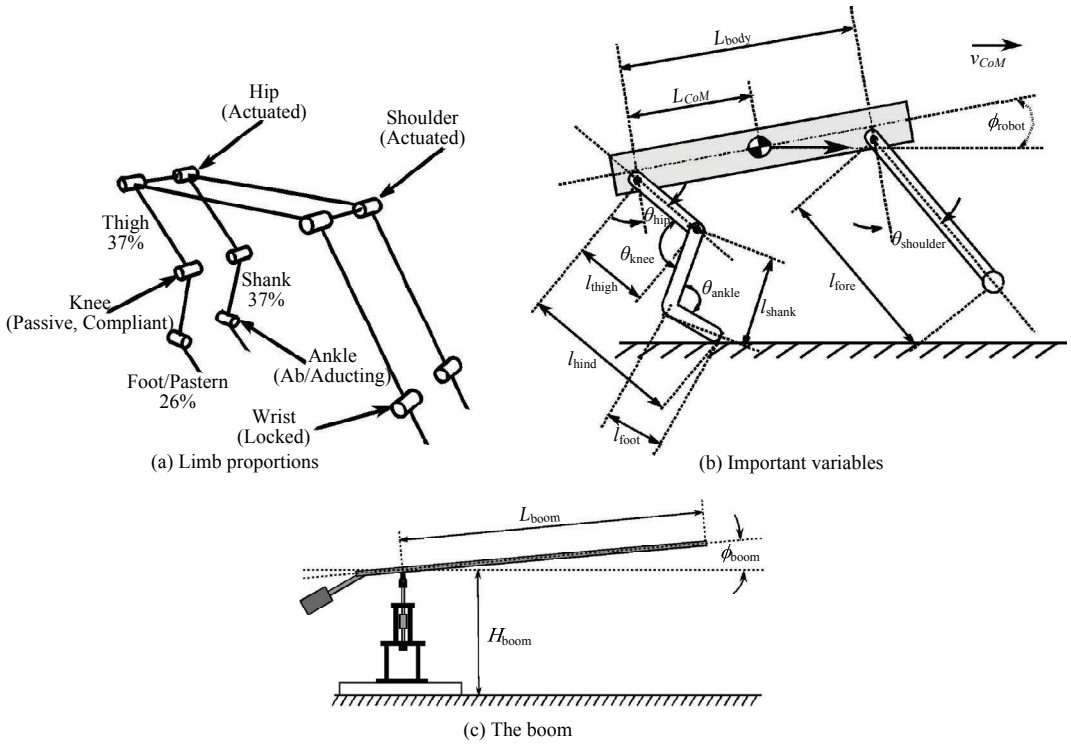

(a) Limb proportions (b) Important variables

(c) The boom

Fig. 2 Important robot geometry and canine-inspired limb proportions in (a) and (b). The angle for the ankle is 131°, while the knee rest angle is 142°. The boom's variables are shown in (c).

The robot was designed in form and function relating to that of real canines. Bioinspiration is derived from partner expertise in the EU FP7 Locomorph project and is size-constrained to permit convenient air transport. The hind leg of the robot had to resemble the hind leg on a small canine and walking performance would be compared with this leg arranged with the knee pointing anteriorly (like the dog it was inspired by) versus posteriorly. Using canine data[33], proportions of the robot's hind limb were established:

(1) The effective straight-line length of the hind leg, l_{hind}, would be approximately 30 cm.

(2) The unloaded knee angle, θ_{knee}, would be 142° with respect to the thigh.

(3) The fixed ankle angle, θ_{ankle}, would be 131° with respect to the shank.

(4) The thigh and shank would be approximately the same length.

(5) If l_{hind}, $l_{shank,}$ and l_{foot} were summed to 100%, then l_{thigh} and l_{shank} would represent approximately 37% each, and l_{foot} would represent approximately 26%.

The hind legs of GARP-5 were designed with three degrees of freedom: one actuated hip, one passive knee and one actuated ankle, shown in Fig. 2a. The hip and knee rotate in the sagittal plane (the plane of forward locomotion), while the ankle rotates in the parasagittal plane. All driving force is generated at the hip motor, and compliance in the leg is at the knee. The focus on actuation at only the hip is inspired by the fact that many quadrupeds, including canines, have the largest proportion of muscle mass devoted to hip-driven movements[34]. GARP-5 is similar in this regard to a large number of other robots[16,35,36]. Foot-stubbing is solved by having the ankle rotate perpendicularly to the hip's plane of motion to effectively shorten the leg for a clear forward swing. Since the ankle is active in only the plane perpendicular to that of hip rotation/knee flexion, the active ankle does not contribute to the forward walking motion of the robot; it simply shortens effective height of the leg to avoid foot-stubbing during protraction.

To support the goal understanding the role of hind leg performance on walking the front legs were simplified. The front legs were simplified to be straight members (no knee and ankle) with wheels fitted on the distal ends (instead of feet, to approximate low friction). The front legs were locked in position for all the tests to keep the robot from tipping over, but also to have little to no effect on the dynamics of the robot (thereby completely isolating dynamic effects to those caused by the hind legs).

2.1 Knee compliance linearization

A monoarticular leg spring was placed about the passive knee to ensure its stability. This acted as an extensor muscle-tendon and ensured that the knee rested at 38° from the thigh's axis. The spring is analogous to the vastus medialis and vastus lateralis muscles, acting as monoarticular knee extensors[37]. The spring constant at the knee was 11 kN·m^{-1} and was chosen experimentally as it permitted the leg to be stiff while the robot stood but complied slightly when compressed by hand, approximating loading during walking. Subsequent locomotion trials with both leg configurations, discussed here, showed that the system could walk. This trial and error approach for the determination of compliance value is normal in legged robotics[36,38–40]. The knee extensor spring, due to constraints for placement of insertion and origin points on the leg mechanism, had to be placed diagonally across the frontal plane of the knee joint as shown in Fig. 3. This led to a nonlinear stretching of the prismatic spring as the knee rotates. The distance, L_{ext}, from the origin to the insertion points, located on the thigh and shank, is written as:

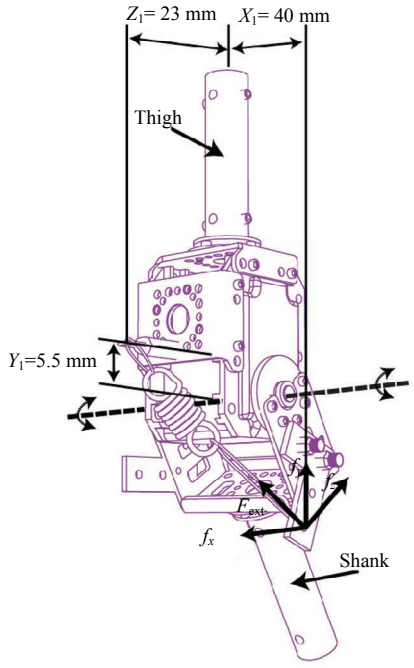

Fig. 3 The hind leg's knee joint, with prismatic leg spring mounted to act as a torsional spring.

$$L_{\text{ext}} = \sqrt{(y_1 + r\cos(\theta))^2 + z_1^2 + (x_1 + r\sin(\theta))^2}, \quad (1)$$

where r is the radius of the arm extending from the knee's revolute joint to the insertion point on the shank, y_1, x_1 and z_1 are the distances along the y, x and z axes between the revolute join and the origin of the spring, located on the thigh. The force developed by this spring is directly proportional to its length, L_{ext}, and its spring constant, k_{ext}, as per Hooke's Law. This results in an expression for prismatic spring force, F_{ext}:

$$F_{\text{ext}}=k_{\text{ext}}L_{\text{ext}}, \quad (2)$$

with components along the x, y and z axes, f_x, f_y, f_z, respectively:

$$f_x=k_{\text{ext}}(x_1+r\sin(\theta)), \quad (3)$$

$$f_y=k_{\text{ext}}(y_1+r\cos(\theta)), \quad (4)$$

and

$$f_z= k_{\text{ext}}z_1, \quad (5)$$

which, in turn, leads to a new expression for F_{ext}:

$$F_{\text{ext}} = \sqrt{f_x^2 + f_y^2 + f_z^2}. \quad (6)$$

This spring force causes a force to be felt tangentially about the knee joint, $F_{\tan}$, which results in a moment about the knee joint, τ_{ext}. The force along the z axis is parallel to the joint and can be ignored because it does not apply a torque to the joint. Therefore τ_{ext} is defined as:

$$\tau_{\text{ext}} = rF_{\tan} = r(f_x\cos(\theta) - f_y\sin(\theta)). \quad (7)$$

Given that the knee was not expected to bend more than 10°, it was decided to represent it as a linearized torsional spring from 38° to 48°, with an assumption of a resting condition at 38°. From Eq. (1) and values of x_1= 40 mm, y_1 = 5.5 mm, z_1= 23 mm and r = 38 mm we determined that the knee spring shown in Fig. 3 would have a 76.2 mm resting length. At 48°, using Eqs. (3) and (4), we obtain forces f_x= 71.1 N and f_y = 66.3 N applied to the shank's insertion point. This yields a torque of 3.68 Nm, according to Eq. (7). Therefore, the linearized spring constant for the knee extensor torsional spring, $k_{\tau_{\text{ext}}}$, is:

$$k_{\tau_{\text{ext}}} = (3.68\ \text{Nm} - 0\ \text{Nm})/(48^{\circ} - 38^{\circ}) = 0.368\ \text{Nm}\cdot\text{deg}^{-1}. \quad (8)$$

2.2 Normal and transverse-mirrored leg configurations

The normal and transverse-mirrored leg configurations are illustrated in Figs. 1a and 1b, respectively. The normal leg is most reflective of canine hind leg morphology (the knee points forward, or cranially), while the transverse-mirrored configuration is achieved by taking the normal leg and turning it around (the knee points backwards, or posteriorly).

A special foot assembly, shown in Fig. 4, permits switching of a leg between the two configurations, each with its own effective leg axis, shown in Fig. 5. From observations in experiment and simulation, the contact surface for the foot was different when walking in either the normal or transverse-mirrored leg configurations. For the normal configuration, contact happens on the plantar surface. For the transverse-mirrored configuration, contact happens on the distal surface.

The Dual Orthogonal Sensing foot design shown in Fig. 4a acts as a hybrid structural and sensing component[41], using two sensors to sense ground contact on the plantar and distal planes of the foot. It is comprised of a Phidgets Inc. 3134 micro load cell and an Interlink Electronics Inc. 2.54 cm diameter circular force sensitive resistor mounted at the tip of the load cell, along the load cell's non-sensitive axis. The load cell was responsible for measuring contact on the plantar plane of the foot (while in normal leg configuration), and the force sensitive resistor was responsible for measuring forces

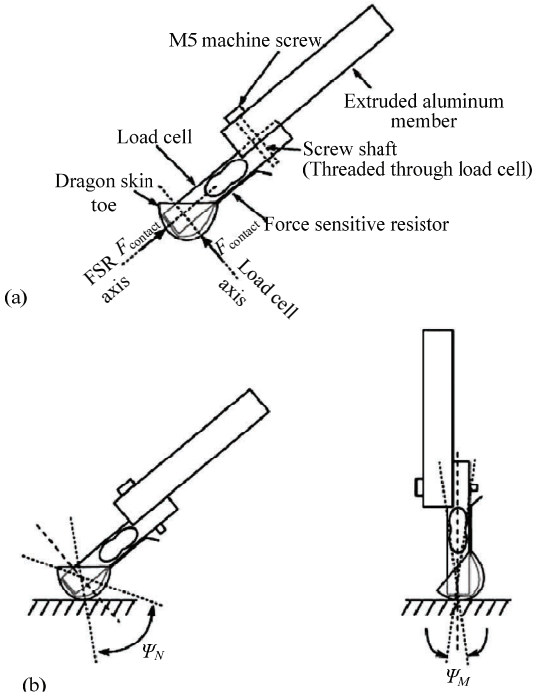

Fig. 4 Hind toe's components and force axes(a) and visualization of contact ranges (b).

on the distal plane (while in transverse-mirrored leg configuration). Since both sensors have different geometries and characteristics, the range of angles of contact for which a touch-down would be registered was limited and unique. This is shown in Fig. 4b where ψ_N and ψ_M are the contact angles for the normal and transverse-mirrored leg configurations, respectively. The range of ψ_N was found to be larger than ψ_M. With the load cell being flat, smooth and metallic, a rounder contact surface with higher friction was needed at the distal end of the foot. Smooth-On Inc. Dragon Skin®, a two-part silicone rubber compound was used to cast the distal end of the load cell into an ovoid with a 3 cm equatorial diameter, cut along the equatorial plane.

The ground contact sensors are used in a binary fashion to determine whether or not the leg is contact with the ground. While mechanical switches could be used instead of load cells and force-sensitive resistors, it is impossible to tune the threshold of most mechanical switches. In contrast, the load cell and force-sensitive resistor sensitivity thresholds can be tuned in software in response to the compliance conditions of the toe or ground. This is the same reason the Scout II, Scorpion, and PAW robots used potentiometers for ground contact rather than switches[42].

2.3 Polynomial trajectory generation

Trajectories for the hip-actuators needed to be generated for the robot to emulate walking motions. These trajectories needed to be non-periodic so that they could be driven by the state-machine (discussed in the next section). Smooth trajectories do not disturb any resonance modes of the mechanical system, so steep first (velocity), second (acceleration), and even third (jerk) derivatives of the motion profiles are avoided in planning the movement of robots[43]. The 7-6-5-4 polynomial trajectory achieves smooth movement for each of the legs. The trajectories were used to make the legs reciprocate, much like a canine leg and are mathematically summarized below:

$$P(\Gamma) = -20\Gamma^7 + 70\Gamma^6 - 84\Gamma^5 + 35\Gamma^4, \qquad (9)$$

where $P(\Gamma)$ is the position trajectory and Γ corresponds to normalized time (from 0 to 1).

Given that the nature of this study was to analyze performance results, a real-time hip angle motion and body pitch motion were not gathered; a time-slice by time-slice comparison of energetics was not the interest. Small changes in contact dynamics can have a large change in moment-to-moment joint trajectories and energetics. These variations however, over a large period of time and number of trials tend to be less significant. More meaningful are the general trends that emerge in variation of the desired hip angles and the comparison of one leg morphology to another.

2.4 High-level gait state-machine

The walking gait of the robot was controlled by a state-machine that coupled the movement of both hind legs. The state-machine was of the Moore type, where outputs relied purely on the current state rather than current state and current inputs[44].

The state-machine can be defined by the variables $\boldsymbol{S_n}$, $\boldsymbol{S_i}$, $\boldsymbol{\lambda}$, $\boldsymbol{\Lambda}$, T, G, where:

(1) $\boldsymbol{S_n}$ is the current state

(2) $\boldsymbol{S_i}$ is the initial state

(3) $\boldsymbol{\lambda}$ is the set of inputs to the state-machine

(4) $\boldsymbol{\Lambda}$ is the output of the state-machine

(5) T is the transition function such that T: $\boldsymbol{S_n} \times \boldsymbol{\lambda} \rightarrow \boldsymbol{S_n'}$

(6) G is the output function such that G: $\boldsymbol{S} \rightarrow \boldsymbol{\Lambda}$

In GARP-5's walking state-machine the input

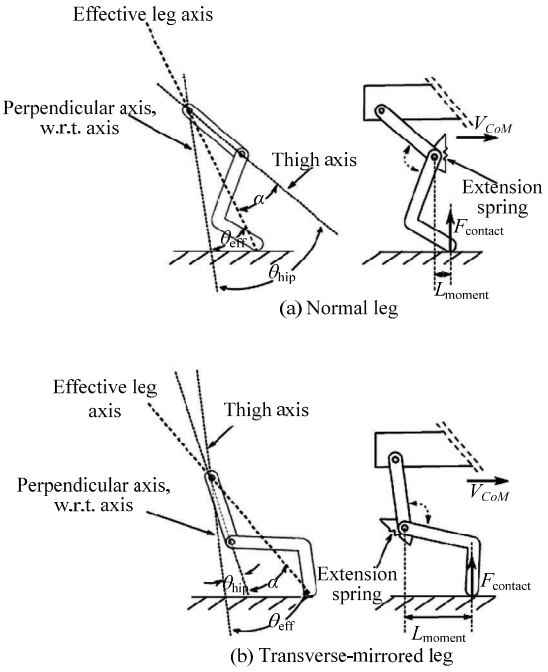

Fig. 5 Effective leg geometry for the normal configuration (a) and transverse-mirrored leg configurations (b). The toe-to-knee moment arm, L_{moment} in (b) is much larger than in (a) for a typical step.

vector is $\boldsymbol{\lambda}=\{TD_3,TD_4\}$, where TD_3 and TD_4 are binary values representing whether the rear left (leg 3) or the rear right leg (leg 4), respectively, has made ground contact (TD_x=1) or not (TD_x=0). The output states are $\boldsymbol{\Lambda}=\{S_n, hold_1, hold_2, action_1, action_2\}$.

The robot starts in state $\boldsymbol{S_i}$, which is a stance taken by the robot at the start of every run. The state-machine transitions out of the initial state by timer into the $action_1$ state, where retraction of leg 4 and protraction of leg 3 occur. Once the two legs hit their end point, the state-machine settles into the $hold_2$ state where both legs hold at the end points of their respective trajectories. Once touch-down is sensed on leg 3 (TD_3), the $action_2$ state occurs and leg 3 is retracted while leg 4 is protracted. The state-machine then settles into the $hold_1$ state. During each *action* state, it is possible for the machine not to reach any *hold* states and transition between the two *action* states if appropriately triggered.

3 Simulation

The GARP-5 robot was simulated in Matlab-Simulink, with the canine-inspired dimensions listed in Table 1. The simulation was used to examine walking in regular and transverse-mirrored leg configurations, shown in Figs. 6a and 7a. The main body parts (*e.g.* central body, thigh, foot, *etc*.) are considered to be uniformly dense masses. Their individual mass values were found by dismantling the robot and weighing each part. A boom is used in this model, as it was on the robot. The front legs have sliding contacts with vertical ground reaction, but no horizontal plane friction to approximate the rolling wheels of the actual robot. The model has abducting/adducting hind feet, just as the robot does. These feet have a switchable ground contact model that engages when the feet penetrate a predetermined plane approximating ground. The ground contact model was a simple linear spring-damper[45], with the vertical component is described as a non-linear spring damper:

Table 1 Geometric nomenclature of the GARP-5 robot and its boom

Parameter	Value
L_{body}	42 cm
W_{body}	18 cm
L_{CoM}	21 cm
l_{hind}	29.5 cm
l_{thigh}	12 cm
L_{fore}	32 cm
l_{shank}	12.3 cm
L_{foot}	8 cm
α	11.2°
L_{boom}	1.17 m

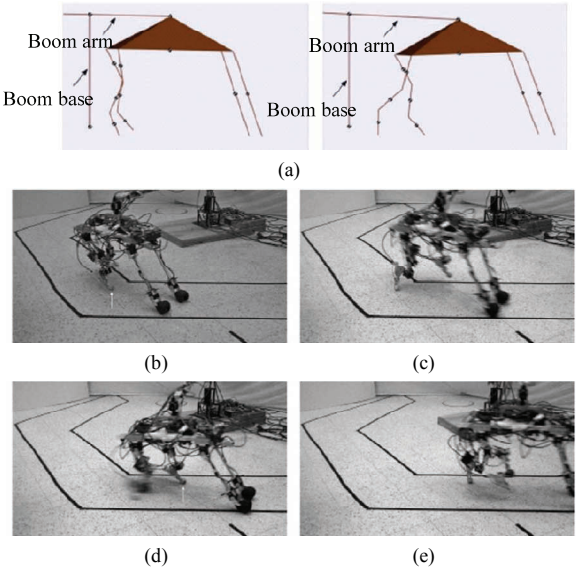

Fig. 6 Normal leg configuration step sequences, in simulation and in experiment. (a) Normal hind leg (simulation), taking two steps; (b) right-hind leg makes contact; (c) right-hind leg pushes back; left-hind leg swings forward; (d) left-hind leg makes contact; (e) left-hind leg pushes back; right-hind leg swings forward.

$$F_n = k\delta + \varsigma\frac{\mathrm{d}\delta}{\mathrm{d}t}, \tag{10}$$

where F_n is vertical ground reaction force, k is the spring constant (set to 500 kN·m^{-1}), ς is the damping constant, and δ is the penetration depth. The damping constant ς is 50 Ns·m^{-1}. The two horizontal components are each defined as piecewise functions:

$$\mu(v)=\begin{cases}\mu_k & :v<-0.00015\,\mathrm{m\cdot s^{-1}}\\ -(\mu_s-\mu_k)\left(\dfrac{0.00015-v}{0.00005}\right)-\mu_k & :-0.0001>v>-0.00015\,\mathrm{m\cdot s^{-1}}\\ -10000v\mu_s & :0>v>-0.0001\,\mathrm{m\cdot s^{-1}}\\ 10000v\mu_s & :0<v<0.0001\,\mathrm{m\cdot s^{-1}}\\ (\mu_s-\mu_k)\left(\dfrac{0.00015-v}{0.00005}\right)+\mu_k & :0.0001<v<0.00015\,\mathrm{m\cdot s^{-1}}\\ \mu_k & :v>0.00015\,\mathrm{m\cdot s^{-1}}\end{cases} \tag{11}$$

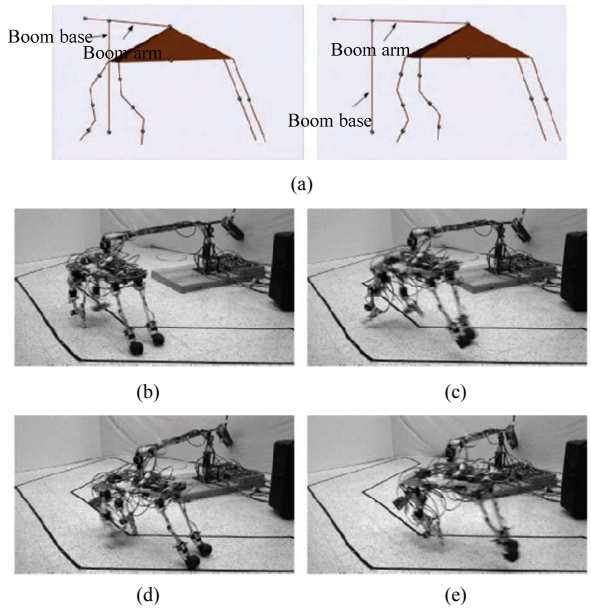

Fig. 7 Transverse-mirrored leg configuration step sequences, in simulation and in experiment. (a) Transverse-mirrored hind leg (simulation), taking two steps; (b) right-hind leg makes contact; (c) right-hind leg pushes back; left-hind leg swings forward (notice the aerial phase achieved by both hind legs; (d) left-hind leg makes contact; (e) left-hind leg pushes back; right-hind leg swings forward.

where μ_s and μ_k are the coefficients of static and kinetic friction, and v refers to either v_x or v_z, the velocities along the x and y axes (in $\mathrm{m \cdot s^{-1}}$). Using this contact model the robot model walked in the normal and transverse-mirrored configurations (Fig. 6a and Fig. 7a). To understand the effect played by the leg configuration on walking performance a series of parameter sweeps were performed on the robot model.

4 Experimental results compared to simulation

Here we describe experiments which confirmed the observations in simulation that the transverse-mirrored configuration is more energy efficient. Screen shots and video stills of the robot and simulation are shown in Figs. 6 and 7. We focus on behaviors and trends in data to ensure that the robot results were not an artifact of the experimental setup. To help ensure this, the robot was made to walk ten times per experimental setting. Power measurements were taken by separately measuring current and voltage of the system during each trial. These values were then used to calculate specific resistance. This was compared to specific resistance values generated directly from simulation results.

A summary of the experimental data is given in Table 2 and Table 3. Lift-off (LO) angle refers to the position of either hind leg once the stance phase of a step was completed. Touch-down (TD) angle refers to the desired position that the either hind leg was held at in the cranial direction readying it to make contact with the ground. Velocity and specific resistance values were the

Table 2 Normal leg experiments summary

TD angle (°)	LO angle (°)	Velocity (average; $\mathrm{m \cdot s^{-1}}$)	Specific resistance (average; unitless)
43	−56	0.3	5.3
43	−27	0.31	5.1
43	12	0.31	5.3
43	11	0.25	6.4
49	−56	0.25	6.2
49	−39	0.27	5.9
49	−27	0.33	5.1
49	−9	0.31	5.1
55	−56	0.27	6.4
55	−42	0.24	6.5
55	−27	0.29	5.6
55	−20	0.29	5.4
61	−56	0.18	8.9
61	−53	0.2	8.0
61	−50	0.23	6.8
61	−47	0.22	7.4

Table 3 Transverse-mirrored leg experiments summary

TD angle (°)	LO angle (°)	Velocity (average; $\mathrm{m \cdot s^{-1}}$)	Specific resistance (average; unitless)
−9	−71	0.39	4.4
−9	−61	0.36	4.1
−9	−50	0.32	4.6
−9	−40	0.29	5.1
−6	−71	0.4	3.9
−6	−61	0.36	4.3
−6	−50	0.32	4.7
−6	−40	0.29	5.2
−4	−71	0.31	4.1
−4	−61	0.31	5.1
−4	−50	0.24	6.8
−4	−40	0.21	7.2
2	−71	0.28	6.4
2	−68	0.17	5.9
2	−65	0.23	5.8
2	−62	0.24	6.3

average values calculated for each set of ten trials. Anything past the boundaries in the tables for either configuration led to instability or inability to locomote.

In Fig. 8, the velocities and specific resistances found in simulation and experiment are compared. Areas of correspondence are highlighted. A good qualitative correspondence was found, as is evident from the shift in TD and LO angles in simulation with respect to the experimental results. This is usual in legged robotics due to the fact that it is impossible to perfectly simulate the real world ground contact conditions[35,40,42,46,47]. Overall, there is a valid qualitative match between the trends seen in simulation and those in experiment.

By inverting the hind leg from normal to transverse-mirrored, the fundamental geometry of the leg with respect to the forward direction of motion changes. Hip angles at LO and TD that worked in the previous geometry don't necessarily work for two reasons: static instability and different areas of contact for the two foot sensors. The result is that some of the hip angles would simply lead to the robot falling over, while others cannot be detected by the toes' sensors. Therefore other LO and TD angles are required. The swapping of the leg direction creates a new morphology that lead to a new, higher level of performance. This is due to two inter-related factors: a new set of LO and TD angles and the engagement of the knee spring[14] showed how both LO and TD angle selection could change bounding speed of a robot and Alexander showed that springs are vital in achieving fast locomotion[48]. Both occur simultaneously to make a generally faster and more efficient gait.

4.1 Specific resistance analysis

Specific resistance is a quantity of measure to compare efficiencies of vehicles as a function of their average velocities[49,50]. It is a unit-less measure that is defined by:

$$\varepsilon(v)=\frac{P(v)}{mgv}, \tag{12}$$

where v is the velocity of the vehicle, $P(v)$ is the total power expenditure with respect to velocity, m is the mass of the vehicle and g is gravitational acceleration. The specific resistance was analyzed for the average velocities obtained for each set of TD and LO angles.

Specific resistance results are shown in Fig. 9a for both simulation and experiment with the normal hind leg configuration, showing similar trends in both. In both cases Fig. 9a clearly shows that as the LO angle becomes more negative (meaning the robot kicks further back) and the TD increases (robot takes a larger step forward), the specific resistance increases. The highest experimental specific resistance found in this configuration was approximately 8.9, and the lowest was approximately 5.1. Similarly, a good qualitative match in the velocity trend is shown between simulation and experiment for the normal leg configuration, as illustrated in Fig. 9b. In both cases, if the TD angle is increased too far towards the front of the robot it yields a braking action that decreases the velocity and increases specific resistance. In experiment a maximum average velocity of 0.33 $m\cdot s^{-1}$ and a minimum average velocity of 0.18 $m\cdot s^{-1}$ were reached. So for the normal leg configuration, qualitative matches in specific resistance and velocity between simulation and experiment were observed.

While we also see a qualitative match between experiment and simulation for the transverse-mirrored hind leg in Fig. 10, the trends in gait are very different than for the normal leg. The results for experiment and simulation in the region which most closely matches the experiments are very similar to the bounding running results reported for the PAW quadrupedal robot: forward speed in running could be increased and specific resistance decreased by sweeping the leg further back during stance[14].

The conclusions can be drawn that the experimental

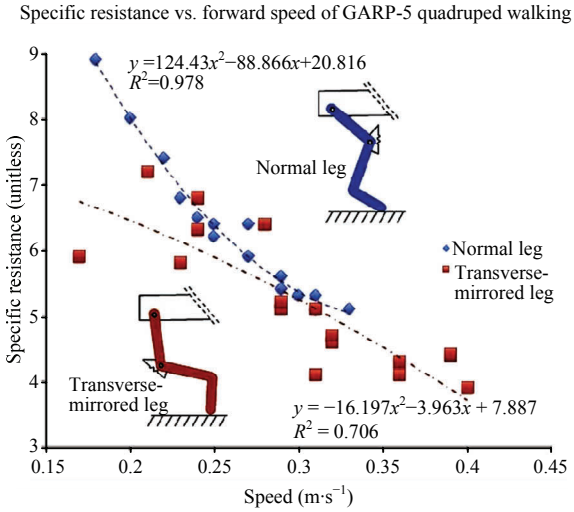

Fig. 8 The walking gait using the transverse-mirrored legs tends to yield more efficient (smaller specific resistance) walking for a given walking speed, as well as giving higher overall speeds than the normal leg. Each data point is the average of ten separate trials.

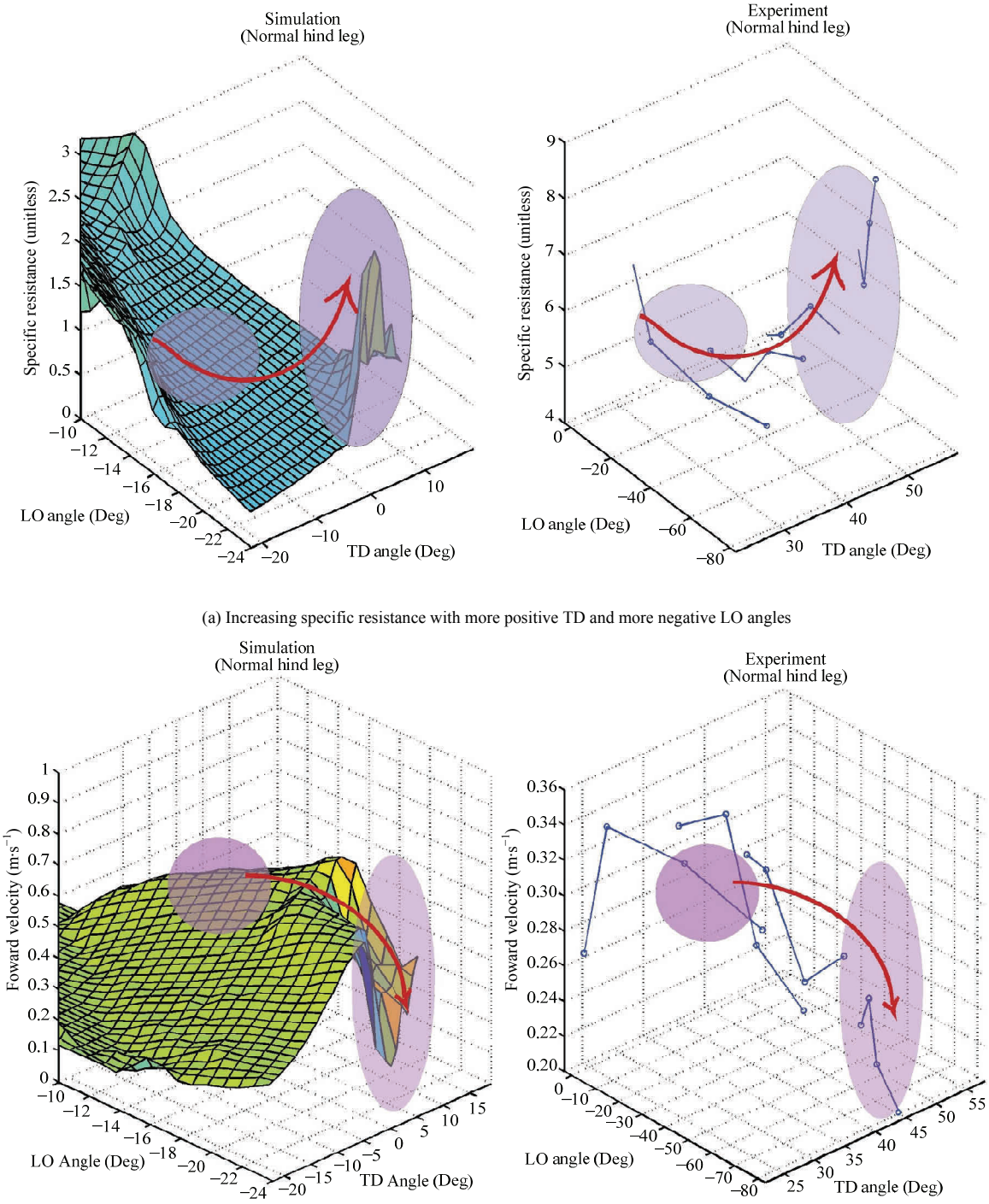

(a) Increasing specific resistance with more positive TD and more negative LO angles

(b) Decreasing velocity with more positive TD and more negative LO angles

Fig. 9 Normal leg configuration simulations (left) versus experiments (right). As the touch-down angles increase towards the front of the robot, specific resistances increase and velocities drop dramatically, illustrating a decrease in efficiency in both simulation and experiment due to braking action by the hind leg.

results qualitatively match the simulation both for normal and transverse-mirrored leg configurations. Furthermore, the transverse-mirrored configuration results closely resemble running the results of a quadrupedal robot[14]. Therefore, there is a possibility that, in general, the transverse-mirrored configuration yields natural dynamics that more closely resemble a running-like gait, as opposed to the gait seen in the normal leg configuration that better resembles a walk. The reason for this difference is tied to how and what degree the knee spring engages in either leg configuration.

It has been noted that changes in body or leg

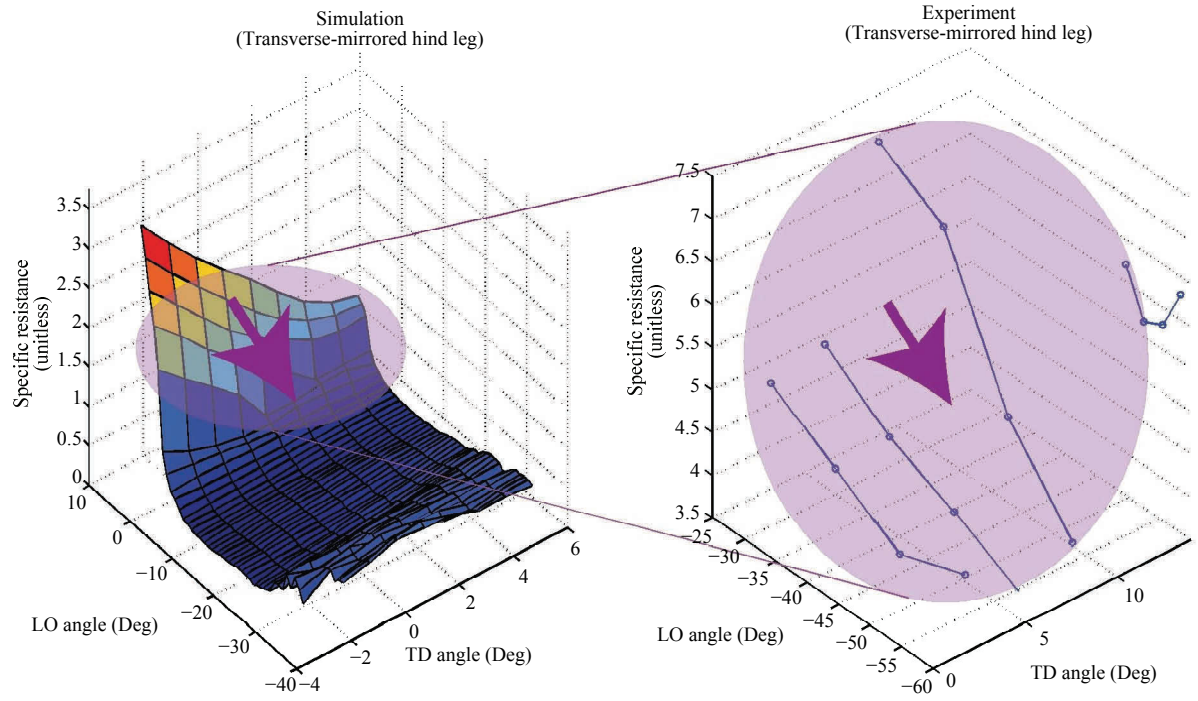

(a) Specific resistance decreasing with decreased LO angle

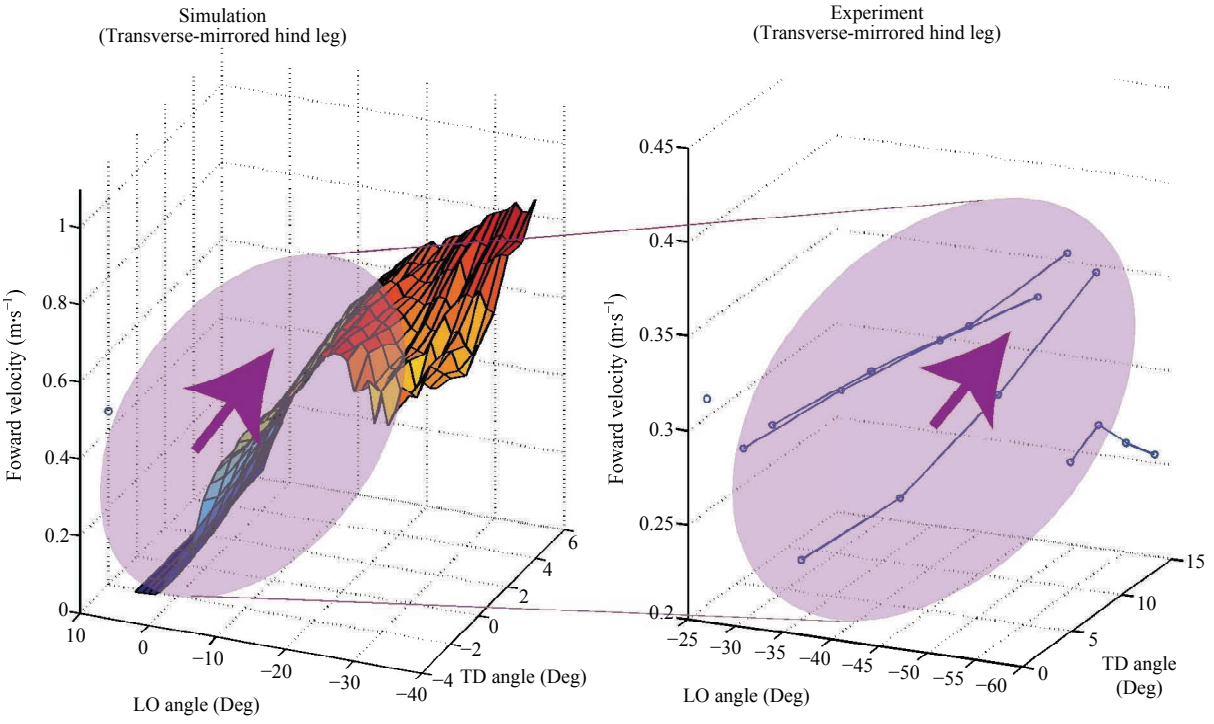

(b) Velocity increasing with decreased LO angle

Fig. 10 Transverse-mirrored leg configuration, simulation (left) versus experiment (right): for most touch-down angles, any decrease in lift-off angle (*i.e.* towards the hind of the robot) yielded an increase in speed and a decrease in specific resistance. This is similar to results for running on the PAW quadrupedal robot[14].

configurations can influence the natural dynamics and locomotory performance[51,52]. In this study we observed a requirement for using different ranges of leg angles for different configurations, due to changes in the robot's natural dynamics[1–4] imposed by the use of two different leg configurations. The two different leg configuration geometries lead the robot to be unstable in certain circumstances for one leg configuration while it would

remain stable with the other. The result is that regardless of the difference in leg trajectories, the performance of the robot as a whole is different when it uses one leg configuration instead of the other.

4.2 The knee spring effect in normal and transverse-mirrored leg configurations

The transverse-mirrored configuration is typically more efficient and achieves higher speeds than the normal leg configuration, as shown in the velocity versus specific resistance curves of Fig. 8. At 0.25 $m \cdot s^{-1}$, both leg configurations yield approximately the same specific resistance. However, the transverse-mirrored configuration is able to achieve higher overall velocities and is more efficient at these velocities than any normal leg walking configuration.

It was observed that the knee compressed much more during the transverse-mirrored walking trials. The knee flexed less than five degrees in the normal leg configuration trials, while flexion up to 20 degrees was observed in the transverse-mirrored leg trials. As shown in Fig. 5, at leg TD the L_{moment} is greater in the transverse-mirrored trials. Therefore, at TD and during the early stage of stance more energy is stored in the knee spring. This energy is released at the end of stance, resulting in a much more energetic gait, capable of achieving higher speed. As seen in Fig. 7b the robot is shown to achieve a modest aerial phase of both hind legs. This is the direct result of the increased spring engagement seen in the transverse-mirrored configuration. In absolute terms, the performance is similar to that of tripod-walking RHex, which also demonstrated energy recovery in its compliant legs during walking[53].

5 Conclusions

We demonstrated that deviating from the kinematics of the animal that inspired a robot leg design can produce faster, more efficient performance. The less biomimetic transverse-mirrored hind leg configuration was more energy efficient and able to attain faster walking velocity than the biomimetic normal hind leg configuration. The lowest overall experimental specific resistance, 3.9, was found in the transverse-mirrored configuration. Experimentally, the fastest average forward walking velocity for the transverse-mirrored configuration was approximately 0.4 $m \cdot s^{-1}$. This study shows that the transverse-mirrored configuration, which more fully engages the knee springs due to the larger L_{moment} between toe and knee, should be selected if speed and energy efficiency are important factors to the robot designer.

Acknowledgment

The authors would like to thank Joel Ramjist for proof-reading this manuscript, as well as Ronnie Wong, Martin Gross, Daniel Renjewski, Sten Grimmer, Andre Seyfarth, Peter Aerts, Rolf Pfeifer, Kasper Stoy, Auke Ijspeert and our other partners in the EU FP7 Locomorph project for engineering, scientific and technical support. We would also like to thank Jason Naughton, Kathryn Atwell, and Alykhan Neky. This work was supported financially by the Natural Sciences and Engineering Research Council (NSERC) of Canada and by Ryerson University's Office of the Vice President of Research and Innovation, and the Department of Electrical and Computer Engineering.

References

[1] Poulakakis I, Smith J A, Buehler M. Modeling and experiments of untethered quadrupedal running with a bounding gait: The Scout II robot. *International Journal of Robotics Research*, 2005, **24**, 239–256.

[2] Geyer H, Seyfarth A, Blickhan R. Natural dynamics of spring-like running: Emergence of self-stability, 5*th International Conference on Climbing and Walking Robots* (*CLAWAR*), Paris, France, 2002.

[3] Ahmadi M. *Stable Control of a One-Legged Robot Exploiting Passive Dynamics*, PhD thesis, McGill University, Montreal, Quebec, Canada, 1998.

[4] Full R J, Kubow T, Schmitt J, Holmes P, Koditschek D. Quantifying dynamic stability and maneuverability in legged locomotion. *Integrative and Comparative Biology*, 2002, **42**, 149–157.

[5] Zhang Z G, Fukuoka Y, Kimura H. Adaptive running of a quadruped robot using delayed feedback control. *Proceedings of the IEEE International Conference on Robotics and Automation* (*ICRA*), Barcelona, Spain, 2005, 3750–3755.

[6] Rummel J, Iida F, Seyfarth A. Enlarging regions of stable running with segmented legs. *Proceedings of the IEEE International Conference on Robotics and Automation* (*ICRA*), Pasadena, California, USA, 2008, 367–372.

[7] Palmer L R, Orin D E, Marhefka D W, Schmiedeler J P, Waldron K J. Intelligent control of an experimental articulated leg for a galloping machine. *Proceedings of the IEEE*

International Conference on Robotics and Automation (*ICRA*), Taipei, China, 2003, 3821–3827.

[8] Nichol J G, Palmer L R, Singh S P N, Orin D E, Waldron K J, System design of a quadrupedal galloping machine. *International Journal of Robotics Research*, 2004, **23**, 1013–1027.

[9] Iida F, Gomez G J, Pfeifer R. Exploiting body dynamics for controlling a running quadruped robot. *Proceedings of the* 12*th International Conference on Advanced Robotics* (*ICAR*), Seattle, USA, 2005, 229–235.

[10] Semini C. *HyQ – Design and Development of a Hydraulically Actuated Quadruped Robot*, PhD thesis, University of Genoa, Genoa, Italy, 2010.

[11] Seyfarth A, Geyer H, Blickhan R, Lipfert S, Rummel J, Minekawa Y, Iida F. Running and walking with compliant legs, in M. Diehl, K. Mombaur (Eds.), *Fast Motions in Biomechanics and Robotics-Optimization and Feedback Control*, Springer Verlag, Berlin Heidelberg, Germany, 2006, 383–401.

[12] Xiuli Z, Haojun Z, Xu G, Zhifeng C, Liyao Z. A biological inspired quadruped robot: structure and control. *Proceedings of the International Conference on Robotics and Biomimetics* (*ROBIO*), Hong Kong, China, 2005, 387–392.

[13] Guan X, Zheng H, Zhang X. Biologically inspired quadruped robot Biosbot: Modeling, simulation and experiment. *Proceedings of the* 2*nd International Conference on Autonomous Robots and Agents*, Palmerston North, New Zealand, 2004, 261–266.

[14] Smith J A, Poulakakis I, Trentini M, Sharf I. Bounding with active wheels and liftoff angle velocity adjustment. *International Journal of Robotics Research*, 2009, **29**, 414–427.

[15] Raibert M. Trotting, pacing and bounding by a quadruped robot. *Journal of Biomechanics*, 1990, **23**, 79–90.

[16] Seyfarth A, Tausch R, Stelzer M, Iida F, Karguth A, von Stryk O. Towards bipedal running as a natural result of optimizing walking speed for passively compliant three-segmented legs, *Proceedings of the* 9*th International Conference on Climbing and Walking Robots* (*CLAWAR*), Brussels, Belgium, 2006.

[17] Wang X, Li M, Guo W, Wang P, Sun L. Velocity control of a bounding quadruped via energy control and vestibular reflexes. *Journal of Bionic Engineering*, 2014, **11**, 556–571.

[18] Li M, Jiang Z, Wang P, Sun L, Ge S S. Control of a quadruped robot with bionic springy legs in trotting gait. *Journal of Bionic Engineering*, 2014, **11**, 188–198.

[19] Ho T, Choi S, Lee S. Development of a biomimetic quadruped robot. *Journal of Bionic Engineering*, 2007, **4**, 193–199.

[20] Giguere S, Dudek G, Prahacs C, Saunderson S. Environment identification for a running robot using inertial and actuator cues. *Proceedings of the Robotics*: *Science and Systems II*, Philidelphia, USA, 2006.

[21] Zhang J, Gao F, Han X, Chen X, Han X. Trot gait design and CPG method for a quadruped robot. *Journal of Bionic Engineering*, 2014, **11**, 18–25.

[22] Maus M. *Stabilisierung Des Oberkoerpers Beim Rennen Und Gehen*, Diploma thesis, Friedrich-Schiller-Universitaet Jena, Jena, Germany, 2008. (in German)

[23] Ringrose R. Self-stabilizing running. *Proceedings of the IEEE International Conference on Robotics & Automation*, Albuquerque, USA, 1997, 487–493.

[24] Schmiedeler J, Waldron K. The mechanics of quadrupedal galloping and the future of legged vehicles. *International Journal of Robotics Research*, 1999, **18**, 1224–1234.

[25] Marhefka D W, Orin D E, Schmiedeler J P, Waldron K J. Intelligent control of quadruped gallops. *IEEE/ASME Transactions on Mechatronics*, 2003, **8**, 446–456.

[26] Li Y, Li B, Ruan J, Rong X. Research of mammal bionic quadruped robots: A review. *Proceedings of the IEEE Conference on Robotics*, *Automation and Mechatronics* (*RAM*), Qingdao, China, 2011, 166–171.

[27] Raibert M H. *Legged Robots That Balance.* MIT Press, Cambridge, USA, 1986.

[28] Hurst J, Rizzi A. Series compliance for an efficient running gait. *IEEE Robotics & Automation Magazine*, 2008, **15**, 42–51.

[29] Chevallereau C, Gabriel A, Aoustin Y, Plestan F, Westervelt E, De Wit C C, Grizzle J. Rabbit: A testbed for advanced control theory. *IEEE Control Systems Magazine*, 2003, **23**, 57–79.

[30] Renjewski D, Seyfarth A. Robots in human biomechanics – a study on ankle push-off in walking. *Bioinspiration & Biomimetics*, 2012, **7**, 036005.

[31] Smith J A, Seyfarth A. Elastic leg function in a bipedal walking robot. *Proceedings of the XXI Congress of the International Society of Biomechanics*, *International Society of Biomechanic*s, Taipei, China, 2007.

[32] Yang T, Westervelt E, Serrani A, Schmiedeler J P. A framework for the control of stable aperiodic walking in underactuated planar bipeds. *Autonomous Robots*, 2009, **27**, 277–290.

[33] Fischer M S, Lilje K E, Lauströer J, Andikfar A. *Hunde in Bewegung*, Franckh Kosmos Verlag, Stuttgart, Germany, 2011. (in German)

[34] Williams S B, Wilson A M, Rhodes L, Andrews J, Payne R. Functional anatomy and muscle moment arms of the pelvic

limb of an elite sprinting athlete: The racing greyhound (canis familiaris). *Journal of Anatomy*, 2008, **213**, 361–372.

[35] Poulakakis I, Smith J A, Buehler M. Experimentally validated bounding models for Scout II quadrupedal robot. *Proceedings of the International Conference on Robotics and Automation*, New Orleans, USA, 2004, 2595–2600.

[36] Moore N. *Leg Design and Stair Climbing Control for the RHex Robotic Hexapod*, Masters thesis, McGill University, Montreal, Canada, 2002.

[37] Hug F, Dorel S. Electromyographic analysis of pedaling: A review. *Journal of Electromyography and Kinesiology*, 2009, **19**, 182–198.

[38] Grizzle J, Hurst J, Morris B, Park H W, Sreenath K, Mabel, a new robotic bipedal walker and runner. *Proceedings of the American Control Conference*, St. Louis, Missouri, USA, 2009, 2030–2036.

[39] Goldman D, Komsuoglu H, Koditschek D. March of the Sandbots. *IEEE Spectrum*, 2009, **46**, 30–35.

[40] Slatton A, Ding Y, Umbanhowar P B, Goldman D, Haynes G C, Komsuoglu, Koditschek D E, Cohen D. Integrating a hierarchy of simulation tools for legged robot locomotion, [2008-08], http://repository.upenn.edu/cgi/viewcontent.cgi?article =1513&context=ese_papers

[41] Chuah M Y, Kim S, Enabling force sensing during ground locomotion: A bio-inspired, multi-axis, composite force sensor using discrete pressure mapping. *IEEE Sensors Journal*, 2014, **14**, 1693–1703.

[42] Smith J A. *Galloping*, *Bounding and Wheeled-Leg Modes of locomotion on Underactuated Quadrupedal Robots*, PhD thesis, McGill University, Montreal, Canada, 2006.

[43] Angeles J. *Fundamentals of Robotic Mechanical Systems - Theory*, *Methods*, *and Algorithms*, 2nd Edition, Springer-Verlag, Berlin Heidelberg, Germany, 2002.

[44] Roth Jr C, Kinney L. *Fundamentals of Logic Design*, Cengage Learning, Boston, USA, 2013.

[45] Gilardi G, Sharf I. Literature survey of contact dynamics modeling. *Mechanism and Machine Theory*, 2002, **37**, 1213–1239.

[46] Morris B, Westervelt E R, Chevallereau C, Buche G, Grizzle J W. Achieving bipedal running with RABBIT: Six steps toward infinity, *Proceedings of Robotics Science and Systems*, Boston, USA, 2005.

[47] Wu T Y, Yeh T J, Hsu B H. Trajectory planning of a one-legged robot performing a stable hop. *International Journal of Robotics Research*, 2011, **30**, 1072–1091.

[48] Alexander R M. Three uses for springs in legged locomotion. *International Journal of Robotics Research*, 1990, **9**, 53–61.

[49] Gabrielli G, von Karman T H. What price speed? Specific power required for propulsion of vehicles. *Mechanical Engineering*, 1950, **72**, 775–781.

[50] Yong J, Smith R, Hatano L, Hillmansen S. What price speed – revisited. *Ingenia*, 2005, **22**, 46–51.

[51] Herr G, Huang G, McMahon T A. A model of scale effects in mammalian quadrupedal running. *Journal of Experimental Biology*, 2002, **205**, 959–967.

[52] Bullimore S, Burn J. Distorting limb design for dynamically similar locomotion. *Proceedings of the Royal Society B*: *Biological Sciences*, 2004, **271**, 285–289.

[53] Neville N. *Bipedal Running with One Actuator per Leg.* Master's thesis, McGill University, Montreal, Canada, 2005.